Multiple extrema in the intermolecular potential and the phase diagram of protein solutions

Simon Brandon,[1,2] Panagiotis Katsonis,[1] and Peter G. Vekilov[1,*]
[1]*Department of Chemical Engineering, University of Houston, Houston, Texas 77204, USA*
[2]*Department of Chemical Engineering, Technion-IIT, Haifa 32000, Israel*
(Received 29 July 2004; revised manuscript received 17 March 2006; published 26 June 2006)

Recent experiments have revealed several surprising features of the phase equilibria in protein solutions: liquid-liquid phase separation which is, in some cases, metastable with respect to the liquid-solid equilibrium, and in others—unobservable; widely varying crystallization enthalpies, including completely athermal crystallization; the co-existence of several crystalline polymorphs; and others. Other studies have shown that the solvent molecules at the hydrophobic and polar patches on the protein molecular surfaces are structured, introducing repulsive forces at surface separations equal to several water molecule sizes. In search of a causal link between the latter and former findings, we apply Monte Carlo simulation techniques in the investigation of phase diagrams associated with globular biological molecules in solution. We account for the solvent structuring via short-range isotropic two-body intermolecular potentials exhibiting multiple extrema. We show that the introduction of a repulsive maximum or a secondary attractive minimum at separations longer than the primary attractive minimum has dramatic effects on the phase diagram: liquid-liquid separation curves are driven to lower or higher temperatures, the sensitivity of the solubility curve (liquidus) to temperature, i.e., the enthalpy of crystallization, is significantly reduced or enhanced, metastable liquid-liquid separation may become stable and vice versa, and both low- and high-density crystalline phases are observed. The similarity of these features of the simulated phase behavior to those observed experimentally suggests that at least some of the mysteries of the protein phase equilibria may be due to the structuring of the solvent around the protein molecular surfaces. Another conclusion is that at least some of the dense liquids seen in protein solutions may be stable and not metastable with respect to a solid phase.

DOI: 10.1103/PhysRevE.73.061917 PACS number(s): 87.15.Nn, 02.70.Uu, 64.70.Dv, 81.10.Dn

INTRODUCTION

Aqueous solutions typically exhibit ordering on the length scale of several water molecules in the vicinity of solid surfaces, including the surfaces of large solute molecules or suspended particles [1,2]. This is especially important in the context of biological macromolecular systems (e.g., protein solutions) in which such solvent structuring is added to the action of a number of interaction forces (van der Waals, double layer, etc.) [3]. The combination of forces has been shown to lead to nontrivial two-body interaction potentials, involving multiple extrema [3–6]. While water structuring and the associated repulsive and more complex intermolecular interaction potential were initially postulated and tested for smooth solid surfaces, e.g., mica [7], both flat and curved, there is ample evidence that water is structured around protein molecules, that the thickness of the structured water layer is significantly greater than the roughness of the protein molecular surfaces [2,5,8], and that solvent structuring modifies the potential of interactions of the protein molecules with surfaces and between pairs of protein molecules [3,4,6,9]. These modifications are adequately modeled by the introduction in the interaction potentials of a repulsive maximum at separations between the protein molecular surfaces equal to several water sizes, i.e., longer than the separation for the attractive minimum underlying the formation of condensed phases: crystals, fibers, gels, dense liquids, etc. [3,4,10–12].

At the same time, a number of features of the phase behavior of protein solutions are still not well understood. These include the insensitivity of solubility of the crystals of many proteins to variations in temperature [13], widespread polymorphism [14], the *lack* of stable or metastable liquid-liquid separation in certain cases [15–17], and other thermodynamic and kinetic effects. Some of the features of the protein phase diagram, such as the variability of the gap between the liquidus and the liquid-liquid separation line, have been correlated with anisotropic intermolecular interactions in a previous Monte Carlo investigation [18]. However, anisotropy cannot be the only factor underlying the specificity of protein phase diagrams: the data in Refs. [13,16,17] were obtained with ferritin and lumazine synthase, proteins with near-spherical symmetry [19,20].

Several groups of previous theoretical works use assumptions similar to ours. In the first group, one or more maxima were added to potentials, in which the attractive minimum is at separations from the particle surface comparable to the particle size. These potentials lead to unique clustering behavior [21,22] (see also Refs. [23–25]). Other studies explored the consequences of similarly modified potentials on pattern formation in colloidal systems confined at the air-water interface [26,27]. In another group of papers, steps in the repulsive term of the square well potential were predicted to dramatically impact the phase diagram of small-molecule liquids [28–30], bringing them to those seen with cesium and cerium [28,29], or phosphorus [30]. Shorter range single extremum potentials have been used in simulations of classical protein phase behavior [31,32]. The addition a single longer range maximum to a short attractive range potential has been

*Corresponding author. Electronic address: vekilov@uh.edu

tested for their consequences for the clustering behavior [33–35], for the gelation and percolation transition [36], and for a phase diagram in coordinates (repulsion strength, temperature) [37], while its consequences for the liquid-liquid, liquid-solid, and solid-solid equilibria of such systems have not been probed. This last group of studies differs from the investigations presented here: it relies on the assumption that the range of repulsion is significantly longer than the range of attraction and comparable to the particle size—in this way the effects of electrostatic double-layer field were modeled [33–37]. With proteins, especially in solutions of ionic strengths higher than 0.1 M, the ranges of intermolecular interactions are significantly shorter than the size of the molecules [31,32]. For ionic strengths close to the physiological 0.10–0.15 M, the characteristic Debye length κ^{-1} is between 9 and 6 Å [38] and even shorter at higher ionic strengths typically used in protein crystallization. Thus the electrostatic double-layer interactions are less important for protein molecules in solution and the shorter range repulsive maximum, due to structuring of the solvent, is more important.

Here, we use Monte Carlo simulations to address the consequences of multiple extrema for phase equilibria in protein solutions. In solutions of different proteins, the maxima and minima in the interaction potential likely vary in number, relative size, and position, and these variations may be of substantial importance. We begin to probe the consequences of multiple extrema by focusing on the effects on phase equilibria of just one repulsive maximum or one secondary minimum in the potential. Since we simulate the behavior of proteins in solution, the attractive minimum is separated from the particle surface by a fraction of the particle diameter; since we assign the longer range repulsion to water structuring, the repulsive maximum is separated from the minimum again by a fraction of the particle diameter. We do not consider nonadditive multiple body effects or temperature-dependent potentials. Although no experimental evidence exists for their significance in protein intermolecular interactions, it is likely that they will affect the protein phase diagram. Thus our approach can yield at best semiquantitative correspondence to the experimentally determined protein phase diagrams. Still, our results suggest that some of the poorly understood phenomena listed above may be at least partially explained by multiple extrema in spherically symmetric interaction potentials.

The simulations below also address the issue of the source of metastability of the liquid-liquid phase separation in protein solutions. Interaction potentials with short widths of attraction have been predicted to lead to the appearance of metastable liquid-liquid separation within the region of stable two-phase liquid-solid coexistence (e.g., Ref. [31] and references within). Metastable liquids have indeed been observed with several proteins [39–42]. It has been claimed that the specific shape of the potential is not important and that the appearance of metastability may be predicted based almost solely on the width of attraction of the potential [18,43]. Our results below indicate that with more complex potentials the width of attraction is not an absolute predictor. Furthermore, we show that certain potentials with short attraction widths may in fact correspond to *stable* liquid-liquid coexistence.

METHODS

As a basis for analysis we use the α potential introduced in Ref. [32] as a model for short-range interactions characterizing protein solution systems. Our modified version of this potential is given by

$$V(r)=\begin{cases}\infty & r\leqslant\sigma\\ \dfrac{4\varepsilon}{\alpha^2}\left\{\dfrac{1}{[(r/\sigma)^2-1]^6}-\dfrac{\alpha}{[(r/\sigma)^2-1]^3}\right\} & \sigma<r<r^*\\ \dfrac{4\varepsilon}{\alpha^2}\left\{\dfrac{1+\gamma[(r/\sigma)^2-(r^*/\sigma)^2]^2}{[(r/\sigma)^2-1]^6}-\dfrac{\alpha}{[(r/\sigma)^2-1]^3}\right\} & r>r^*\end{cases}, \tag{1}$$

which is composed of a hard-sphere repulsion term for short distances ($r\leqslant\sigma$), the α potential for intermediate distances ($\sigma<r\leqslant r^*$), and an augmented α potential for large distances ($r>r^*$). Here, σ is the hard core diameter, ε is the depth of the primary minimum, α is a parameter determining the range of the potential, and r^* is a distance above which a local repulsive maximum or secondary attractive minimum (depending on the sign of the premultiplier γ) are added. Although the additional term, premultiplied by γ, was originally chosen to mimic the hydration-repulsion effects suggested in Refs. [10,11,44], it is treated in this analysis as an arbitrarily added repulsion or attraction designed to highlight the effects of a generic additional extremum in the potential. Sample potentials, calculated using $\gamma=0$ (standard α potential), $\gamma>0$ (local repulsive maximum), and $\gamma<0$ (secondary minimum) are depicted in Fig. 1.

Liquid-solid and liquid-liquid coexistence curves were evaluated, using, respectively, the Gibbs-Duhem [45,46] and the Gibbs ensemble [47] methods; the Gibbs-Duhem method was, in some cases, used to reproduce liquid-liquid coexistence curves. These methods rely on the search for equilibrium between the respective pairs of phases, with each phase held in a separate "box." With the Gibbs-Duhem method, 108 solid-phase and 128 liquid-phase particles were used in calculations of liquid-solid equilibrium (select liquid-solid coexistence curves were found to require 256 solid-phase

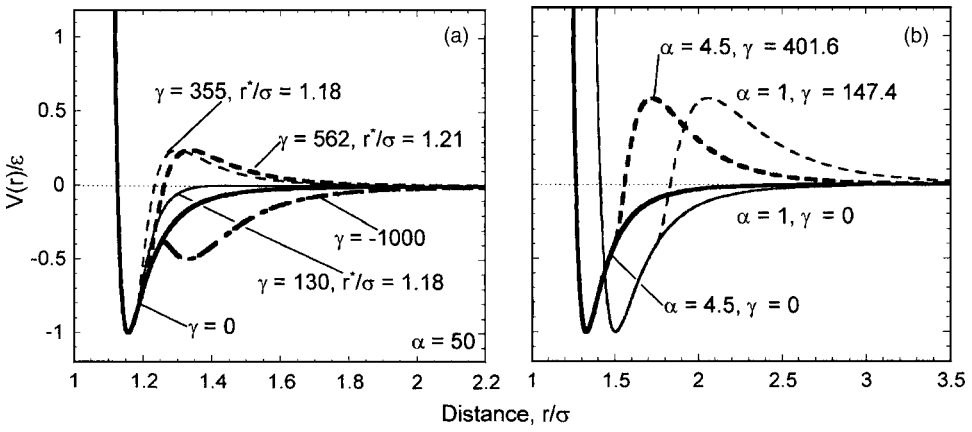

FIG. 1. Intermolecular potentials, with one or two extrema, constructed using Eq. (1) with (a) $\alpha=50$: base case with $\gamma=0$ (thick solid line), $\gamma=130$ and $r^*/\sigma=1.18$ (thin solid line), $\gamma=562$ and $r^*/\sigma=1.21$ (thick dashed line), $\gamma=355$ and $r^*/\sigma=1.18$ (thin dashed line), $\gamma=-1000$ and $r^*/\sigma=1.25$ (thick dash-dotted line); (b) $\alpha=4.5$ and $\gamma=0$ (thick solid line), $\alpha=1$ and $\gamma=0$ (thin solid line); $\alpha=4.5$, $\gamma=401.6$, and $r^*/\sigma=1.5017$ (thick dashed line); $\alpha=1$, $\gamma=147.4$, and $r^*/\sigma=1.7528$ (thick dashed line).

and 250 liquid-phase particles for increased accuracy), 128 particles per phase (256 total) were used when applying this technique to liquid-liquid coexistence calculations, 1372 for the expanded and 500 particles for the dense fcc phases were used for the solid-solid coexistence. The Gibbs ensemble technique employed 256 (or, for tests of system size effects, 400 or 600) particles equally divided between the two phases.

Periodic boundary conditions were used, and the interactions were truncated at distances at which the potential magnitude receded below 0.003ε. On the average, a Monte Carlo (MC) cycle involved one displacement attempt per particle and three volume change attempts; for the Gibbs ensemble technique, an additional 50 particle exchange attempts were made. At each temperature, with the Gibbs-Duhem technique 20–35 kilocycles brought the pressures and chemical potentials of the particles in the two phases to equal values, with overlapping ranges of their intrinsic numerical fluctuations; 25–40 additional kilocycles were typically used for the estimation of the properties of each phase. With the Gibbs ensemble technique, typically 200 kilocycles were needed for mechanical and chemical equilibration and 400 additional kilocycles were used for the estimation of the properties of the two phases in equilibrium.

Liquid-solid coexistence calculations were initiated at high temperatures T (typically $T=10^{13}\varepsilon/k$; k is the Boltzmann constant), at which a noninteracting hard-sphere system was assumed. Integration of the Clapeyron equation using a predictor-corrector method was performed by applying two different versions of this equation, depending on the temperature range [48]. In cases where this method was applied to liquid-liquid coexistence calculations, initial conditions for integration were obtained from results of a Gibbs ensemble simulation.

Varying the value of the parameter α changes, among other things, the thickness of the soft repulsive shell surrounding the hard spherical core of the potential. Similar to Ref. [48], we calculate an effective diameter $\sigma_{\text{eff}}=\int_0^{r_0}\{1-\exp[-V(r)/kT]\}dr$, see Ref. [49], where r_0 is the shortest distance for which $V(r_0)=0$. This σ_{eff}, and the sample number density ρ are used to define a volume fraction $\phi=\pi\rho\sigma_{\text{eff}}^3/6$.

RESULTS AND DISCUSSION

Liquid-liquid separation and the medium range repulsive maximum

As a base case, we chose a system described by the α potential with $\alpha=50$. The phase diagram associated with this typical short-range potential in Fig. 2(a) coincides with those in the literature [32]. Introduction of a repulsive maximum in the potential visibly changes both the liquidus (solubility) and liquid-liquid coexistence curves, Figs. 2(a) and 2(b). The radial distribution function for the solid phase obtained with the potential with a repulsive maximum, as in the base case, indicates the expected fcc structure. The sensitivity of the liquidus to temperature is reduced. The Gibbs-Helmholtz equation for the liquid-solid equilibrium $\Delta H_{L\text{-}S}/kT^2=d\ln K_{L\text{-}S}/dT$, with $\Delta H_{L\text{-}S}$ the enthalpy of the liquid-solid transition (the latent heat of crystallization) and defining the equilibrium constant for crystallization $K_{L\text{-}S}=\phi_{\text{liquidus}}^{-1}$, becomes $\Delta H_{L\text{-}S}/kT^2=-d\ln\phi_{\text{liquidus}}/dT$. This equation shows that the lower temperature sensitivity of the liquidus corresponds to lower magnitude values of the crystallization enthalpy in the whole T range. Thus variations in solvent structuring in solutions of different compositions and the related variations in the intermolecular interaction potential might be the reason for the broad variability of the protein crystallization enthalpy even in cases where a protein crystallizing from different solvents forms similar structures with similar intermolecular contacts [50].

Another observation from Figs. 2(a) and 2(b) is that with the introduction of medium-range repulsion, "hump," the critical point for liquid-liquid coexistence is driven to lower temperatures, i.e., the stability of the liquid-liquid separation

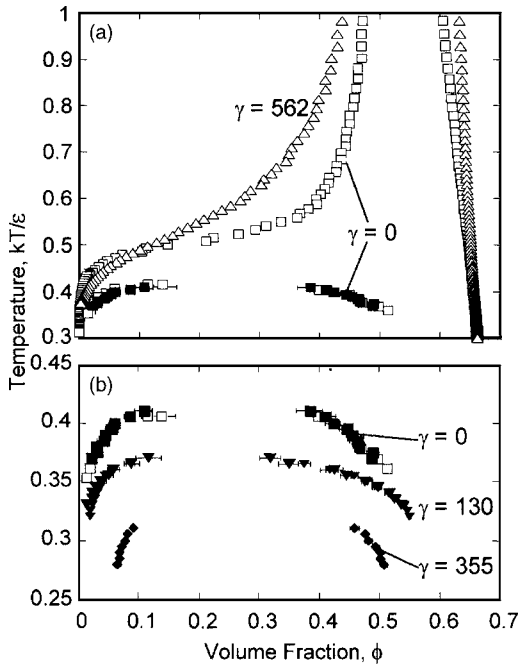

FIG. 2. Liquid-solid and liquid-liquid coexistence associated with the $\alpha=50$ potentials shown in Fig. 1(a). Open symbols denote Gibbs-Duhem results, solid symbols—Gibbs ensemble results. (a) liquid-solid and liquid-liquid coexistence lines for the base-case with $\gamma=0$ (squares); liquid-solid equilibrium lines for $\gamma=562$ and $r^*/\sigma=1.21$ (triangles). (b) Liquid-liquid coexistence lines for base case with $\gamma=0$ (squares), $\gamma=130$ and $r^*/\sigma=1.18$ (inverted triangles), $\gamma=355$ and $r^*/\sigma=1.18$ (diamonds). Different sized inverted triangles refer to different Gibbs ensemble runs.

is further reduced. The stability of the L-L coexistence has been correlated with the characteristics of the interparticle potential: for square-well potentials, the width of the attractive well is a direct predictor of this stability [43]. There is an added complexity for systems with more developed potentials, for which at least two spatial characteristics may be defined. The width of attraction of a potential can be defined as the difference of the distances at which the potential equals half the attraction depth $\varepsilon/2$. With this definition, the width of attraction carries straightforward physical meaning as a measure of the distance at which two approaching particles start to attract. An alternative characteristic, called range of attraction, relies on the equation of the osmotic second virial coefficient of the tested potential with the corresponding square-well potential [51]. Although the range is indirect and temperature dependent, it is a more comprehensive characteristic of the potential: it accounts for the details of the potential shape [51].

Comparing the potentials with and without a hump in Fig. 1(a), we see that the hump leads to shrinking of the width of attraction by ~30%, from 0.0968 for the base-case α potential to 0.068 for the $\gamma=355$ case. Since the range is evaluated via B_{22}, it depends on temperature. The ranges of the potentials at the critical temperatures for L-L coexistence for the systems without and with a hump are 0.074 and 0.035, i.e., the hump reduces the range by ~2×. This is an example where the range of attraction of a potential, which depends on its specific shape, appears to be a more sensitive predictor of the phase behavior than the width, which only characterizes the attractive part. Another example, in which equal widths and different ranges correspond to entirely different phase diagrams, is provided below.

The lower sensitivity of the liquidus line to temperature and the lower temperatures for liquid-liquid phase separation are consistent with observations of the phase behavior of solutions apoferritin and lumazine synthase: the solubilities of the fcc crystals of apoferritin and the hexagonal crystals of lumazine synthase do not depend on temperature [13,17], and no liquid-liquid separation is observed for either protein at temperatures as low as −10 °C, below which the solution freezes and the protein denatures. Apoferritin (point symmetry group m3) and lumazine synthase (point symmetry group 532) molecules are nearly spherical and experiments have shown that potentials of interactions between pairs of molecules of these proteins in solution should contain repulsive maxima similar to those assumed in the simulations above [10–12,17,44].

Crystalline clusters in the liquid phases

In the cases where a potential with a repulsive maximum was used in Gibbs ensemble simulations for temperatures below the critical, convergence as judged by the equality of the pressures and chemical potentials of the particles in the two phases proceeded significantly slower. In some cases, especially with higher repulsive maxima, even after up to 5 megacycles, the ranges of the intrinsic numerical fluctuations of the pressure and chemical potential in the two phases were only partially overlapping, with significant fluctuations and no trend to further convergence. Although the volume fractions at the ends of such runs were very close to other runs with identical assumptions and shown in Fig. 2(b), these results were not plotted there.

To understand the fluctuations and the slight inconsistency of the final volume fractions in some runs, we monitored the phase variations, which take place in both the dilute and dense liquid phases. In the dilute liquid phase, structured aggregates, illustrated by the snapshot in Fig. 3(a), often appear, and dissolve or destructure after a time. These clusters appear in all runs, and because of their limited lifetime, they do not affect the convergence of the simulation runs. The system is at the low-density segment of the liquid-liquid coexistence line, i.e., it is supersaturated with respect to the crystalline phase, and we conclude that the structured aggregates are subcritical crystalline clusters. It is tempting to trace a similarity between these clusters and those predicted and seen in Refs. [33–35]. However, the theoretically assumed [34,35] and experimentally realized [33,34] source of long-range repulsion is the electrostatic interaction, which has a range comparable and longer than the particle diameter. As Fig. 1(a) shows, the "hump" in our simulations extends to only a fraction of that diameter. As a result, in a row of particles the third particle would not feel the first in our system, while for the published systems, even nonneighboring particles would strongly interact. Thus it seems that the mechanism of formation of clusters in our system is

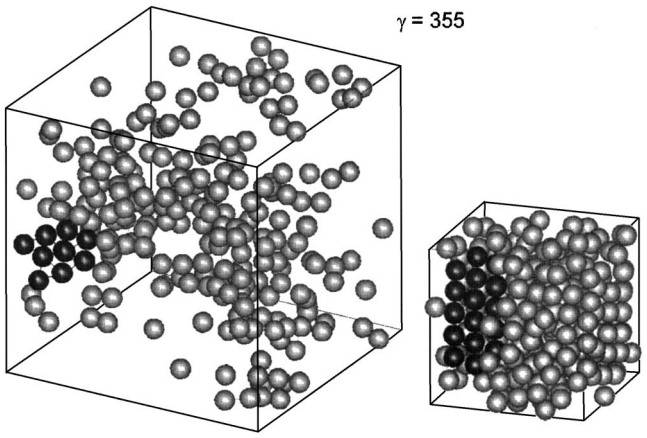

FIG. 3. Snapshots of the two coexisting dense liquid phases that contain 256 particles each, interacting with potentials with $\gamma=355$ and $r^*/\sigma=1.18$, at $T=0.3\varepsilon/k$ after 200 kilocycles of evolution. The darker particles partake an ordered structure, whose upper layer covers particles of the lower layers. In the dilute liquid in (a) these structures are smaller and easily dissolve, while in the dense liquid (b) they are more stable and usually grow.

different form the elegant mechanism put forth in Ref. [25] for systems with electrostatic double-layer repulsion. Since the cluster formation seen in our simulations corresponds to experimental observations [17,52], this mechanism merits detailed considerations.

In the dense liquid phase small crystallites like the one of the Fig. 3(b) emerge and persist as the system evolves in time only in the runs that failed to completely converge. Visual inspection of snapshots such as these in Fig. 3(b) revealed that the crystallites were typically more than one, but the number of particles in them was always a fraction of the total in the dense phase. Significantly, for the base-case potential with $\gamma=0$, such structured clusters were never observed for simulation lengths even an order of magnitude longer than specified in the Methods section.

For quantitative evidence for the presence of such crystalline clusters in the dense liquid phase, we carried out local bond order analysis [53,54]. This type of analysis has two important advantages: it is sensitive to the overall degree of crystallinity, independent of a specific crystal structure, and the bond-order parameters are insensitive to the cluster orientation in the analyzed configuration. We calculated the bond order parameters q_ℓ ($\ell=2$, 4, 6, 8, and 10) for each particle in a simulation volume of interest, for definitions and mathematical expressions of q_ℓ, see Refs. [53,54]. These q_ℓ characterize the symmetry of the "bonds" between a particle and its nearest neighbors; each q_ℓ has a range of typical values for each of the symmetries of the environment of the particle [53,54]. Thus the symmetries of the environments are characterized by the sets of values of q_ℓ. Since the ranges of values of q_6 for disordered, hexagonal, face- and body-centered-cubic environments have relatively low overlap, this parameter is often used to distinguish between the different arrangements of spherical particles [54]. To enhance the resolution between these ranges of q_6, sometimes the vector dot product $q_6(i)\cdot q_6(j)$, where i and j denote two neighboring particles and the vector dot product is computed

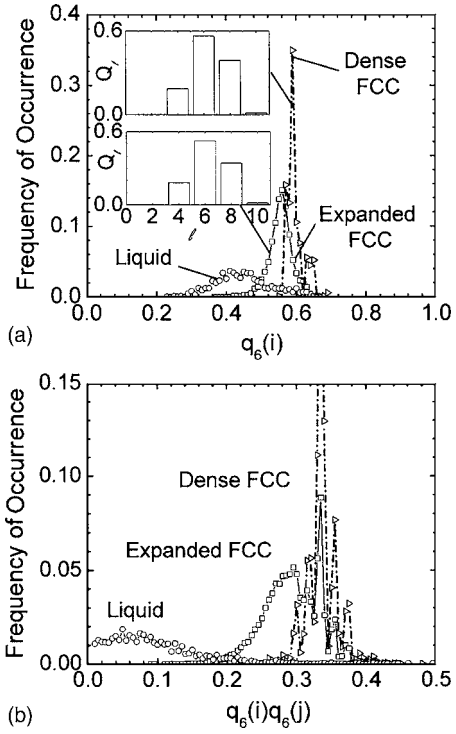

FIG. 4. Local bond order analysis of ○: dense liquid phase for $\gamma=355$ at $\phi=0.53$, see Fig. 2(b); □: expanded solid phase at $\phi=0.59$, see Fig. 5(a); and ▷: dense solid phase at $\phi=0.64$, see Fig. 5(a). (a) Distributions of values of the of the local bond order parameter q_6 for these three systems; insets: values of parameters q_2–q_{10} averaged over entire systems containing expended and dense solid phases. (b) Distributions of the values of the vector dot product $q_6(i)\cdot q_6(j)$ for two nearest-neighbor particles i and j in these three systems.

following a somewhat complex rule, is used [54]. According to its definition, the dot product $q_6(i)\cdot q_6(j)$ is a complex number. The distributions of $\mathrm{Re}[q_6(i)\cdot q_6(j)]$ and $|q_6(i)\cdot q_6(j)|$ are similar and we chose to plot the real part, $\mathrm{Re}[q_6(i)\cdot q_6(j)]$, which in the text and figures below we denote as $q_6(i)\cdot q_6(j)$. Note that the values of $\mathrm{Re}[q_6(i)\cdot q_6(j)]$ can differ significantly from $[q_6(i)]^2$.

In Fig. 4, we show the distributions of $q_6(i)$ and $q_6(i)\cdot q_6(j)$ over all particles in the dense liquid phase volume. While both distributions show maxima at values typical for disordered phases [53,54], both plots contain second shoulders in the q_6 range 0.5–0.7 and the $q_6(i)\cdot q_6(j)$ range 0.2–0.4, which correspond to a significant number of particles in the fcc environments.

The appearance of crystalline aggregates only in the simulations with a repulsive maximum is very interesting: we note that both systems with and without a repulsive maximum are supersaturated with respect to the crystalline phase. In such systems, structural fluctuations towards the stable crystalline phase are always present. These fluctuations are manifest in structured clusters of various sizes and, in general, limited lifetimes. However, the repulsive maximum likely affects the thermodynamics and kinetics of the evolution of the structured clusters. The shorter range of attraction of the hump potential should correlate with a lower energy of

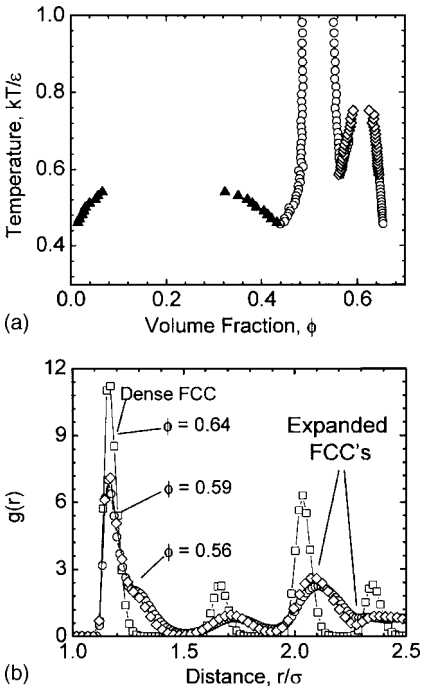

FIG. 5. (a) Liquid-solid (circles), liquid-liquid (triangles), and solid-solid (triangles), and solid-solid (diamonds) coexistence lines for the case with a secondary minimum: $\gamma=-1000$ and $r^*/\sigma=1.25$. Open symbols denote Gibbs-Duhem results, solid symbols denote Gibbs Ensemble results. (b) The radial distribution functions of the three solid phases at temperature $T=0.7\varepsilon/k$. The two expanded fcc phases have almost identical plots.

the unsaturated bonds on a cluster's surface (a microscopic equivalent to lower surface free energy [55]). This should reduce the critical cluster size [55–57] and stabilize the clusters, whose size is greater than this critical value. Furthermore, the repulsive maximum delays the decay of the structure fluctuations (the destructuring of the crystalline clusters) by acting as an activation barrier for the detachment of each particle from a cluster. Both of these phenomena increase the lifetime of the structured clusters, their probability for growth, and their average size. This hypothetical mechanism deserves detailed further investigations that should address, among other issues, the reasons why even when crystals form, they do not capture the whole dense liquid. The considerations above should only be viewed as an intuitive explanation of some of the features observed in the simulations.

Stable dense liquid and polymorphism

Hydration repulsion is only one of a number of possible forces acting in aqueous solutions of biological macromolecules. The combination of these may result in a secondary minimum in the potential [3] such as the one depicted by the dashed-dotted curve in Fig. 1(a). Liquid-solid and liquid-liquid coexistence curves corresponding to this potential are presented in Fig. 5(a). A number of interesting features stand out. Most prominently, the liquid-liquid coexistence is now stable and the likely reason for the increased stability of the liquid-liquid separation is the increased range of attraction for the potential with a secondary minimum. Indeed, the potential with a second minimum tested in these simulations has the same *width* of attraction=0.0968 as the base case α potential, but its range at the critical temperature for L-L coexistence expands almost twofold: from 0.074 for the base case α potential to 0.152. This comparison provides an example of the better predictive power of the potential range than the potential width of attraction. This comparison also shows that the phase behavior depends strongly on details of the interaction potential, such as its shape. The stabilization of the dense liquid observed in Fig. 5(a) suggests that some of the numerous cases of "oiling out" observed in protein solutions [58,59], may in fact represent not metastable, but stable dense liquid phase.

While for high temperatures the liquidus line in Fig. 5(a) conforms to that of the base-case calculation, it deviates from the base case, $\gamma=0$, result at temperatures in the range $(1-0.45)\varepsilon/k$ and ends at a triple point where it meets the liquid-liquid curve. The solidus conforms to that of the base case for temperatures down to $T\cong 15\varepsilon/k$ [this temperature range is above the one displayed in Fig. 5(a)], below which it exhibits significantly lower densities than that of the base case. At a temperature of $T\cong 0.57\varepsilon/k$ this low-density phase becomes unstable and transforms into another solid phase with higher density, Fig. 5(a), resulting in a solid-solid triple point. At temperatures between $0.75\varepsilon/k$ and $0.57\varepsilon/k$ a solid-solid coexistence with a critical point is observed. Similar stable solid-solid transitions have been observed for other systems with a narrow width of attraction that exhibit metastable liquid-liquid transition [59,61]. The potential used here, with a secondary minimum, which is characterized by short width and longer range of attraction presents a rare example of a system where both liquid-liquid and solid-solid transitions are stable.

The radial distribution functions of the three solid phases, shown in Fig. 5(b), show that all of them have fcc structures. However, the first peak for the two lower-density solid phases consists of two partially overlapping peaks. The two constituent peaks correspond to the two potential minima in Fig. 1(a), which may be occupied by the first nearest neighbors, see similar behavior in Refs. [60,61]. Peaks that correspond to farther nearest neighbors appear as smooth and wide, since the two positions become indistinguishable. This radial distribution function indicates that the lower-density solids are partially disordered fcc crystals, in which a particle can be in either of two positions with respect to its nearest neighbors. The conclusion of the partially disordered fcc structure of the expended solid phase is supported by the bond-order distributions. The average values of the q_ℓ's ($\ell=2$, 4, 6, 8, and 10) for both the expanded and dense solids shown in the insets of Fig. 4(a) are typical of fcc symmetry [53,54]. However, the distribution of $q_6(i)$ is broader and shifted to lower values, characteristic of disordered phases; this shift and broadening are even more apparent in the $q_6(i)\cdot q_6(j)$ distribution in Fig. 5(b). Thus the transition from an expanded to a high-density solid is a first-order phase transition between two solids, in which all particles move to the deepest minimum of interactions with their neighbors.

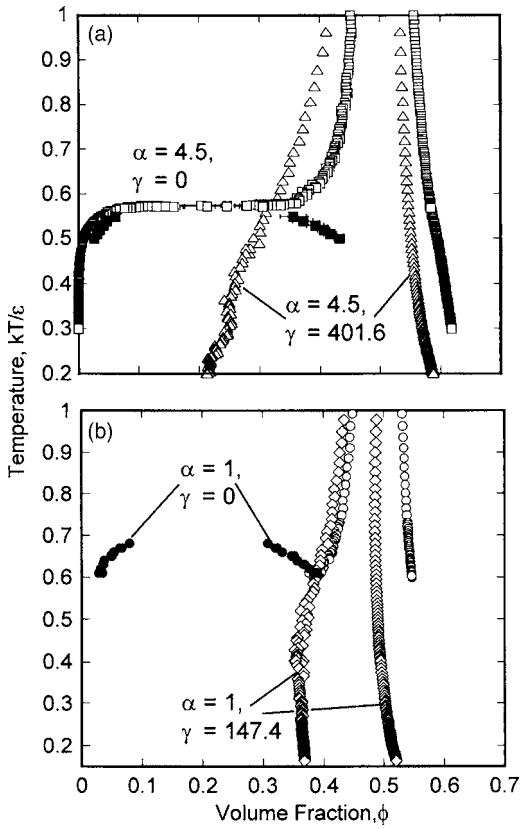

FIG. 6. Temperature T–volume-fraction ϕ phase diagrams for (a) $\alpha=4.5$. Liquid-solid and liquid-liquid coexistence lines for $\gamma=0$ (squares); liquid-solid coexistence for $\gamma=401.6$ and $r^*/\sigma=1.5017$ (triangles). (b) $\alpha=1$. Liquid-solid and liquid-liquid coexistence lines for $\gamma=0$ (circles); liquid-solid coexistence for $\gamma=147.4$ and $r^*/\sigma=1.7528$ (diamonds). Open symbols denote Gibbs-Duhem results; solid symbols denote Gibbs ensemble results.

Metastability of the liquid-liquid coexistence

The metastability of the liquid-liquid coexistence has been explained as a result of the short range of intermolecular attractive interactions. In the context of the α potentials, there exists a critical $\alpha\approx4.5$ below which the liquid-liquid coexistence is stable while above this value metastability is observed. In Fig. 6 we investigate the impact of adding a local repulsive maximum to two different potentials whose parameters differ by the value of α: $\alpha=4.5$ in Fig. 6(a) is sufficiently large for metastability, while $\alpha=1$ in Fig. 6(b) ensures stable liquid-liquid coexistence and a triple point. We see that, as for $\alpha=50$ above, in both cases with the introduction of a repulsive maximum, the liquidus line becomes less sensitive to temperature, with particularly strong consequences for the $\alpha=1$, where at low temperatures the liquidus is essentially vertical. The Gibbs-Helmholtz equation (see above) indicates that in this case the enthalpy of solidification effectively vanishes. The persistence of the Gibbs-Duhem results for the liquid-solid equilibria down to very low temperatures in Figs. 6(a) and 6(b) indicates that the liquid-liquid equilibrium has been pushed to low temperatures and is metastable.

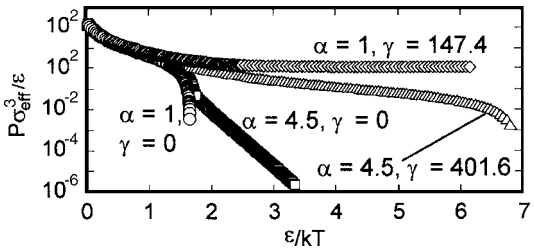

FIG. 7. Pressure P–temperature T plots corresponding to liquid-solid coexistence for $\gamma=0$: $\alpha=4.5$ (squares) and $\alpha=1$ (circles), and for $\gamma\neq0$: $\alpha=4.5$, $\gamma=401.6$, $r^*/\sigma=1.5017$ (triangles); $\alpha=1$, $\gamma=147.4$, $r^*/\sigma=1.7528$ (diamonds).

These conclusions about the transition to metastability and the disappearance of the triple point are supported by the $P(T)$ dependencies in Fig. 7. At very high temperatures, where all systems behave like noninteracting hard spheres, the scaled pressure $P\sigma^3/kT=11.696$ [62] for all four cases. The system with $\alpha=1$ and $\gamma=0$ exhibits a divergence of $\ln(P)$ vs $1/T$ near the triple point, similar to that shown by Lennard-Jones solid-liquid coexistence [46], while the three other systems show a continuous decrease of pressure with decreasing temperature, supporting metastable liquid-liquid coexistence and the lack of triple point. The system with $\alpha=4.5$ and $\gamma=0$ shows a kink in the $P(T)$ curve at a temperature where the volume fraction of the low-density liquid phase rapidly decreases with decreasing temperature [observe open squares at $kT/\varepsilon=0.57$ in Fig. 6(a)]. Finally, the Clapeyron equation, $\Delta H_{L\text{-}S}/T\Delta\phi_{L\text{-}S}=dP/dT$ ($\Delta\phi_{L\text{-}S}$ is the difference in volume fraction ϕ between solid and liquid phases) together with the vanishing slope of $P(T)$ for $\alpha=1$ with a repulsive maximum (diamonds in Fig. 7), strongly suggests, in agreement with the conclusion based on the Gibbs-Helmholtz equation and the slope of the liquidus above, that the enthalpy of crystallization is negligible in this system.

CONCLUSIONS

The results presented here demonstrate that many of the peculiarities of the phase behavior of protein solutions: metastable dense liquid phases, highly variable temperature gap between the solubility and the liquid-liquid coexistence phase lines, lack of liquid-liquid separation in the temperature ranges of protein stability, highly variable in magnitude enthalpies of formation of ordered solid phases, widely spread polymorphism, etc., do not necessarily indicated potentials with short width of attraction [31,63] or the lack of spherical symmetry [18]. We show that these features of the phase diagram may be consequences of an additional maximum or minimum in a spherically symmetric intermolecular interaction potential. As shown in the literature, such additional maxima or minima are due to structuring of the water and other solvent molecules at the surface of the protein molecules.

We also show that a potential that is a realistic representation of the intermolecular interactions in protein solutions

may lead to a dense liquid stable with respect to a solid phase. This result suggests that at least some of the numerous dense liquids seen in protein solutions may be stable and not metastable with respect to a solid phase.

ACKNOWLEDGMENTS

We thank Dimiter N. Petsev for informative discussions of protein phase behavior. This work was supported by the Office of Biological and Physical Sciences, NASA.

[1] J. N. Israelachvili, *Intermolecular and Surface Forces* (Academic, New York, 1995).
[2] S. K. Pal and A. H. Zewail, Chem. Rev. (Washington, D.C.) **104**, 2099 (2004).
[3] D. Leckband and J. Israelachvili, Q. Rev. Biophys. **34**, 105 (2001).
[4] N. Choudhury and B. M. Pettitt, J. Phys. Chem. B **109**, 6422 (2005).
[5] V. A. Makarov, B. M. Pettitt, and M. Feig, Acc. Chem. Res. **35**, 376 (2002).
[6] J. J. Valle-Delgado, J. A. Molina-Bolivar, F. Galisteo-Gonzalez, M. J. Galvez-Ruiz, A. Feiler, and M. W. Rutland, Langmuir **21**, 9544 (2005).
[7] R. M. Pashley and J. N. Israelachvili, J. Colloid Interface Sci. **97**, 446 (1984).
[8] D. I. Svergun, S. Richard, M. H. Koch, Z. Sayers, S. Kuprin, and G. Zaccai, Proc. Natl. Acad. Sci. U.S.A. **95**, 2267 (1998).
[9] D. N. Petsev, B. R. Thomas, S.-T. Yau, and P. G. Vekilov, Biophys. J. **78**, 2060 (2000).
[10] V. Paunov, E. Kaler, S. Sandler, and D. Petsev, J. Colloid Interface Sci. **240**, 640 (2001).
[11] M. Manciu and E. Ruckenstein, Langmuir **18**, 8910 (2002).
[12] P. G. Vekilov and A. A. Chernov, in *Solid State Physics*, edited by H. Ehrenreich and F. Spaepen (Academic, New York, 2002), Vol. 57, p. 1.
[13] D. N. Petsev, B. R. Thomas, S.-T. Yau, D. Tsekova, C. Nanev, W. W. Wilson, and P. G. Vekilov, J. Cryst. Growth **232**, 21 (2001).
[14] A. McPherson, *Preparation and Analysis of Protein Crystals* (Wiley, New York, 1982).
[15] Y. G. Kuznetsov, A. J. Malkin, and A. McPherson, Phys. Rev. B **58**, 6097 (1998).
[16] S. Tanaka and M. Ataka, J. Chem. Phys. **117**, 3504 (2002).
[17] O. Gliko, N. Neumaier, W. Pan, I. Haase, M. Fischer, A. Bacher, S. Weinkauf, and P. G. Vekilov, J. Am. Chem. Soc. **127**, 3433 (2005).
[18] A. Lomakin, N. Asherie, and G. Benedek, Proc. Natl. Acad. Sci. U.S.A. **96**, 9465 (1999).
[19] D. M. Lawson, P. J. Artymiuk, S. J. Yewdall, J. M. A. Smith, J. C. Livingstone, A. Trefry, A. Luzzago, S. Levi, P. Arosio, G. Cesareni, C. D. Thomas, W. V. Shaw, and P. M. Harrison, Nature (London) **349**, 541 (1991).
[20] K. Ritsert, R. Huber, D. Turk, R. Ladenstein, K. Schmidt-Bäse, and A. Bacher, J. Mol. Biol. **253**, 151 (1995).
[21] M. Dzugutov, Phys. Rev. A **46**, R2984 (1992).
[22] J. P. K. Doye, D. J. Wales, F. H. M. Zetterling, and M. Dzugutov, J. Chem. Phys. **118**, 2792 (2003).
[23] J. Groenewold and W. K. Kegel, J. Phys. Chem. B **105**, 11702 (2001).
[24] A. Stradner, H. Sedgwick, F. Cardinaux, W. C. K. Poon, S. U. Egelhaaf, and P. Schurtenberger, Nature (London) **432**, 492 (2004).
[25] F. Sciortino, S. Mossa, E. Zaccarelli, and P. Tartaglia, Phys. Rev. Lett. **93**, 055701 (2004).
[26] S. J. Mejia-Risales, A. Gil-Villegas, B. I. Ivlev, and J. R. Garcia, J. Phys.: Condens. Matter **14**, 4795 (2002).
[27] R. P. Sear, S.-W. Chung, G. Markovich, W. M. Gelbart, and J. R. Heath, Phys. Rev. E **59**, R6255 (1999).
[28] D. A. Young and B. J. Alder, Phys. Rev. Lett. **38**, 1213 (1977).
[29] D. A. Young and B. J. Alder, J. Chem. Phys. **70**, 473 (1979).
[30] G. Franzese, G. Malescio, A. Skibinsky, S. V. Buldyrev, and H. E. Stanley, Nature (London) **409**, 692 (2001).
[31] N. Asherie, A. Lomakin, and G. B. Benedek, Phys. Rev. Lett. **77**, 4832 (1996).
[32] P. R. ten Wolde and D. Frenkel, Science **277**, 1975 (1997).
[33] A. I. Campbell, V. J. Anderson, J. S. v. Duijneveldt, and P. Bartlett, Phys. Rev. Lett. **94**, 208301 (2005).
[34] Y. Liu, W.-R. Chen, and S.-H. Chen, J. Chem. Phys. **122**, 044507 (2005).
[35] S. Mossa, F. Sciortino, P. Tartaglia, and E. Zaccarelli, Langmuir **20**, 10756 (2004).
[36] A. Coniglio, L. D. Arcangelis, E. D. Gado, A. Fierro, and N. Sator, J. Phys.: Condens. Matter **16**, S4831 (2004).
[37] M. Tarzia and A. Coniglio, Phys. Rev. Lett. **96**, 075702 (2006).
[38] M. Muschol and F. Rosenberger, J. Chem. Phys. **103**, 10424 (1995).
[39] J. A. Thomson, P. Schurtenberger, G. M. Thurston, and G. B. Benedek, Proc. Natl. Acad. Sci. U.S.A. **84**, 7079 (1987).
[40] M. Muschol and F. Rosenberger, J. Chem. Phys. **107**, 1953 (1997).
[41] M. Casselyn, J. Perez, A. Tardieu, P. Vachette, J. Witz, and H. Delacroix, Acta Crystallogr., Sect. D: Biol. Crystallogr. **57**, 1799 (2001).
[42] O. Galkin, K. Chen, R. L. Nagel, R. E. Hirsch, and P. G. Vekilov, Proc. Natl. Acad. Sci. U.S.A. **99**, 8479 (2002).
[43] A. Lomakin, N. Asherie, and G. B. Benedek, J. Chem. Phys. **104**, 1646 (1996).
[44] D. N. Petsev and P. G. Vekilov, Phys. Rev. Lett. **84**, 1339 (2000).
[45] D. A. Kofke, J. Chem. Phys. **98**, 4149 (1993).
[46] R. Agrawal and D. A. Kofke, Mol. Phys. **85**, 43 (1995).
[47] A. Z. Panagiotopoulos, Mol. Phys. **61**, 813 (1987).
[48] M. G. Noro and D. Frenkel, J. Chem. Phys. **114**, 2477 (2001).
[49] J. A. Barker and D. Henderson, J. Chem. Phys. **47**, 4714 (1967).
[50] M. Ataka and M. Asai, J. Cryst. Growth **90**, 86 (1988).
[51] M. G. Noro and D. Frenkel, J. Chem. Phys. **113**, 2941 (2000).
[52] O. Gliko, N. Neumaier, W. Pan, I. Haase, M. Fischer, A. Bacher, S. Weinkauf, and P. G. Vekilov, J. Cryst. Growth **275**, e1409 (2005).
[53] P. J. Steinhardt, D. R. Nelson, and M. Ronchetti, Phys. Rev. B

28, 784 (1983).
[54] S. Auer and D. Frenkel, J. Chem. Phys. **120**, 3015 (2004).
[55] R. Kaischew and I. N. Stranski, Z. Phys. Chem. Abt. B **35**, 427 (1937).
[56] J. W. Gibbs, Trans. Conn. Acad. Arts Sci. **3**, 108 (1876).
[57] J. W. Gibbs, Trans. Conn. Acad. Arts Sci. **16**, 343 (1878).
[58] Y. G. Kuznetsov, A. J. Malkin, and A. McPherson, J. Cryst. Growth **232**, 30 (2001).
[59] M. Dijkstra, Phys. Rev. E **66**, 021402 (2002).
[60] P. Bolhuis, M. Hagen, and D. Frenkel, Phys. Rev. E **50**, 4880 (1997).
[61] P. Bolhuis and D. Frenkel, J. Phys.: Condens. Matter **9**, 381 (1997).
[62] W. G. Hoover and F. H. Ree, J. Chem. Phys. **49**, 3609 (1968).
[63] M. H. J. Hagen and D. Frenkel, J. Chem. Phys. **101**, 4093 (1994).